



The Use of a Modified Camera for the Classification of Sedimentary Rocks

CEZARY TOŚ, Cracow, Poland

Keywords: modified camera, classification, sedimentary rocks

Summary: The article presents studies on the possibility of using a modified NIR digital camera to carry out an initial classification of sedimentary rock formations. The study has been conducted in the limestone mine “Czatkowice” in Poland. For this purpose, samples of the formations typical for that deposit have been photographed in four channels: blue (B: 380 nm – 520 nm), green (G: 440 nm – 620 nm), red (R: 560 nm – 720 nm), and near infrared (NIR: 820 nm – 1,100 nm). The recorded images of each of the samples have been compared against the spectral curves prepared on the basis of the studies carried out with a field spectrometer. This comparison has been carried out using earlier prepared sensitivity characteristics for the modified camera. However, in contrast to other NIR devices, the wide sensitivity range in the NIR channel resulted in a lack of a clear spectral peak. The hypothesis about the usefulness of a modified camera in recognition of sedimentary rocks has been verified by analysing the results of the classification of rock samples and a fragment of the quarry wall. This classification has been made using channels in the visible range and in the near infrared. The accuracy of the classification measured by the kappa index of agreement (KIA) has been increased when using the NIR channel. The study indicated that in some cases a modified camera can be a cheaper alternative to professional equipment recording near infrared channel.

Zusammenfassung: Die Nutzung einer modifizierten Kamera zur Klassifikation von Sedimentgesteinen. Dieser Beitrag präsentiert eine Potenzialstudie zur Nutzung einer modifizierten digitalen Nahinfrarotkamera zu einer ersten Klassifikation von Felsformationen am Beispiel des Kalksteinbruchs “Czatkowice” in Polen. Typische die Lagerstätte charakterisierende Gesteinsproben wurden in vier Kanälen aufgezeichnet: blau (B: 380 nm – 520 nm), grün (G: 440 nm – 620 nm), rot (R: 560 nm – 720 nm), und nahes Infrarot (NIR: 820 nm – 1.100 nm). Die aufgezeichneten Bilddaten der einzelnen Proben wurden mit spektralen Profilen aus Aufnahmen mit einem Feldspektrometer verglichen. Dieser Vergleich wurde durchgeführt unter Verwendung der vorgefertigten Empfindlichkeitseigenschaften für die modifizierte Kamera. Durch einen relativ breiten Empfindlichkeitsbereich konnte kein Peak im NIR-Kanal erfasst werden, wie das für andere NIR-Kameras möglich ist. Die Hypothese, dass die modifizierte Kamera sich zur Erkennung von Sedimentgesteinen eignet, wurde durch die Analyse der Klassifikationsergebnisse der Gesteinsproben und einem Ausschnitt der Steinbruchwand verifiziert. Bei dieser Klassifikation wurden verschiedene Kanalkombinationen getestet. Die Genauigkeit der Klassifikation gemessen mit dem Kappa Index of Agreement (KIA) konnte durch die Hinzunahme des NIR channels verbessert werden. Die Ergebnisse zeigen, dass diese einfache Modifikation der Kamera als kostengünstige Alternative zur professionellen NIR-Kamera angesehen werden kann.

1 Introduction

The technique of classifying rocks using multispectral and hyperspectral imaging has been popular for quite some time now. It is conducted to carry out geological research, primarily on the basis of satellite or aerial images. Ground-based equipment is used much more seldom for that purpose. Recently, ground-based hyperspectral cameras have been applied much more frequently and studies are carried out on the possibility of using laser scanners for such classifications. This type of equipment is relatively expensive and difficult in operation.

Commonly used digital cameras register light in the visible range and in three channels, namely red (R: 560 nm – 720 nm), green (G: 440 nm – 620 nm), and blue (B: 380 nm – 520 nm). Introducing a minor modification to a digital camera and using inexpensive filters make it possible to register light in the near infrared range (NIR: 820 nm – 1,100 nm). Using such a modified camera as a research tool for geological applications is a very rare case. For instance, SULISTIYANTI et al. (2009), or SULISTIYANTI et al. (2010) investigated the possibilities of a modified camera to register thermal images. SULISTIYANTI et al. (2014) also used it for the detection of air pollution. Moreover, it was proposed that NIR data could actually prove to be remarkably useful in colour consistency assessment, to estimate the incident illumination, as well as to detect the location of different illuminants (FREDEMBACH & SUSSTRUNK 2009). VERHOEVEN (2008) quotes the possibility of using a modified camera in archaeological research.

This article analyses the suitability of a modified camera to carry out a classification of formations in the wall of the “Czatkowice” Limestone Mine. Today, the assessment of a quarry wall composition and, consequently, of the quality of excavated material, is based on laboratory-based testing of samples and on in situ analysis performed by a geologist. The use of a remote observation technique would significantly facilitate their work, if a geologist had access to a preliminary classification of formations. Employing a simple method of photographing with a modified camera could become such a technique.

2 Digital Camera – Application in Rock Classification and Possibilities of Camera Modification

Physico-chemical properties of rock materials related to the capacity of the minerals to absorb or reflect electromagnetic radiation are the basis of remote sensing methods used in geology. The spectral ranges primarily used in these studies include the visible (VIS), near infrared (NIR) and short-wave infrared (SWIR) ranges. But also mid infrared (MIR) and thermal infrared (TIR) spectral ranges have been utilized (VAN DER MEER et al. 2012). Remote sensing in geology is based on the fact that minerals are characterized by specific absorption of the radiation due to electronic processes in the mineral lattice in the VIS and NIR and by vibrational processes in the SWIR spectral ranges. These processes include, among others, the following: crystal field effects, charge-transfer, colour centres, transitions to the conduction band, and overtone as well as combination tone vibrational transitions (HUNT 1980). The processes in the MIR and TIR spectral ranges include, for instance, volume scattering effects, as well as emissivity and temperature interference. Therefore, a characteristic set of spectral peaks can be defined for the individual minerals in order to enable the identification of the minerals during laboratory tests using spectroscopy.

There are numerous studies in this field, e.g. HUNT (1977) and EDWARDS et al. (2005) on the spectral characteristics of carbonate minerals, on REE fluorocarbonates (Rare Earth Elements) (TURNER et al. 2014), or on mudstone (LIU et al. 2016). Rock formations consist of various minerals with characteristic spectral peaks that may superimpose (BROWN 2006). Also, the shape of the spectral curve is affected by grain size (BALDRIDGE et al. 2009). A larger grain has a greater internal path where photons may be absorbed. Thus, reflectance decreases with increasing grain size. However, using hyperspectral data analysis methods, e.g. band calculation, feature mapping, expert systems or spectral deconvolution, it is possible to determine not only the type of minerals but also their quantity in the rocks (ASADZADEH & DE SOUZA FILHO 2016, KUOSMANEN & LAITINEN 2008, HAEST et al. 2012).

Outside the laboratory, multispectral and hyperspectral imaging at satellite or aircraft levels are used for geological cartography (CIAMPALINI et al. 2012, CHEN et al. 2007, KRUSE 2015, GOETZ 2009). Multispectral imaging often has a reduced capability to identify individual rock formations due to the limited number of recorded spectral channels and a usually lower spectral resolution (GOETZ 2009). However, the use of a small number of channels in combination with the methods of supervised classification makes it possible to distinguish between rock formations without specifying their exact mineral composition, as shown by KOVACEVIC et al. (2009). This can be done if the studied rocks have unique spectral characteristics in the recorded channels. For instance, for the cartography of dolomitic rocks, it is recommended to use three channels (Nos. 6, 8 and 7) in the SWIR range from the ASTER (Advanced Spaceborne Thermal Emission and Reflectance Radiometer) satellite. For carbonates, in turn, it is recommended to use channels of the TIR range (Nos. 13 and 14) or again three channels (Nos. 7, 8 and 9) recorded in the SWIR. Rocks containing iron compounds are easy to identify in images using a combination of channels Nos. 1 and 2 (VIS), 3 (NIR) and 4 (SWIR) (VAN DER MEER et al. 2012).

Digital cameras are devices that enable recording of three spectral channels in the VIS range and, despite their simplicity, they are

also used in geological studies. MENGKO et al. (2000) and PIRARD (2004) use digital cameras with narrow bandwidth interference filters to identify minerals in rocks, NURDAN & NIHAT (2010) apply neural networks based image analysis for the same purpose, and TARQUINI & FAVALLI (2010) determine rock texture on the basis of collimated RGB images. LEPISTO et al. (2005) investigated bedrock properties by analysing the digital images. CHATTERJEE et al. (2010) and PATEL & CHATERIEE (2016) analysed data from a digital camera with supervised classification methods to determine the quality of the limestone used at a cement plant. The use of a digital camera is not limited to laboratory testing. For instance, PENASA et al. (2014), FRANCESCHI et al. (2009) and TOŚ (2014) study the suitability of scanning data including RGB channels and, additionally, intensity of laser beam reflection to classify sedimentary rocks in the working face of a quarry. Those works inspired the author to carry out investigations on the use of a modified camera recording NIR. The NIR channel could complement the scanning data obtained from the laser scanner.

The detector of a digital camera is a matrix of sensors. CMOS (Complementary Metal-Oxide-Semiconductor) or CCD (Charge Coupled Device) sensors are used most commonly. The light-sensitive area, called photodiode, collects photons during the exposure time (NAKAMURA 2006, THEUWISSEN 1995). All detectors applied in both types of sensors register

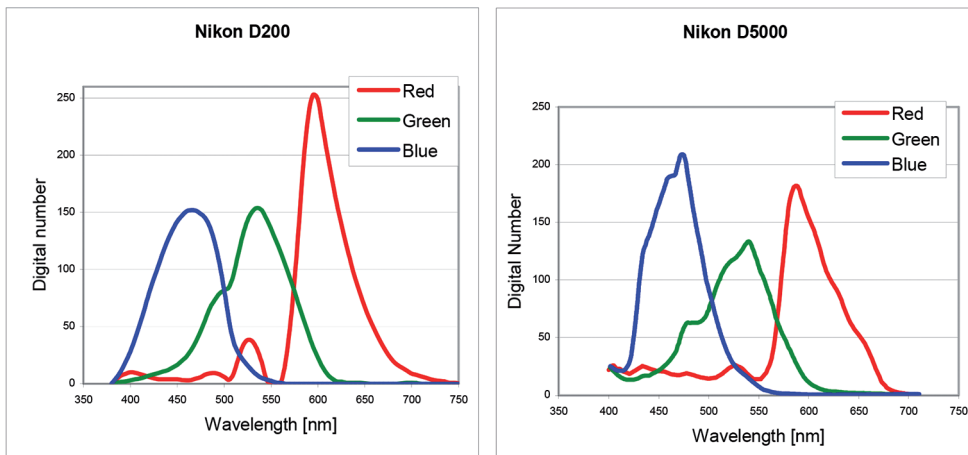


Fig. 1: Spectral sensitivities of: a) Nikon D200 adapted from Image Engineering (NIKOND200 2015), and b) Nikon D5000 adapted from BONGIORNO et al. (2013).

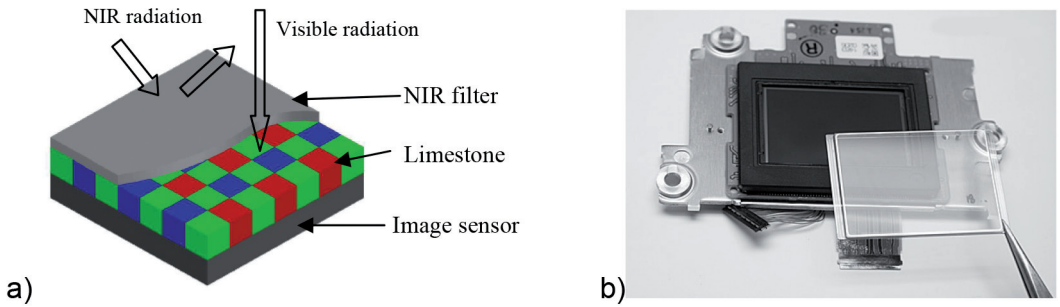


Fig. 2: a) A sensor with Bayer and infrared filters adopted from VERHOEVEN (2008), b) removal of the NIR filter (NIKOND70 2015).

light in the same spectrum. Each sensor contains a system of filters arranged in the form of a checkboard. The checkboard is composed of individual filters each of which transmits light in selected wavelengths. Each of the charge-coupled devices is covered with a single filter, which means that it only registers light of a desired wavelength (NAKAMURA 2006) (Fig. 1). The Bayer filter is an example of such an arrangement (Fig. 2a).

Cameras are equipped with an additional NIR filter installed on the sensor (Fig. 2a), since the Bayer filter does not cut off radiation in the NIR region. The NIR filter factory-installed on the sensor has to be replaced with a different filter that transmits radiation in the full range of sensitivity of charge-coupled devices, in order to increase the camera's sensitivity to infrared radiation. A filter replacement is not complicated. The pro-

cess is depicted in Fig. 2b. When this is done, charge-coupled devices will register radiation in the range from 280 nm to approximately 1,100 nm. The diagram (Fig. 3) demonstrates the adjusted spectral response curves for a Nikon D200 camera in the range 380 nm – 1,000 nm. The diagram has been prepared by LDP LLC (MAXMAX 2015) and presents RGB values of the light coming from a monochromator, registered by the camera. The values have been normalised with the data generated by a spectrometer that measures the frequency and intensity of the light that falls on the sensor (MAXMAX 2015).

When analysing the diagram, one will see that the curves for the R and B values are similar in the range above 850 nm. The G values are much smaller, on the other hand. It is required to use an additional filter on the sensor or on the lens in order for the camera to reg-

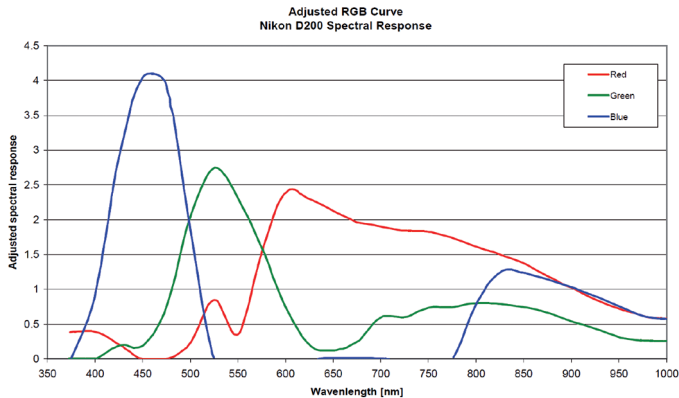


Fig. 3: Nikon D200-adjusted spectral response curves adapted from LDP LLC (MAXMAX 2015).

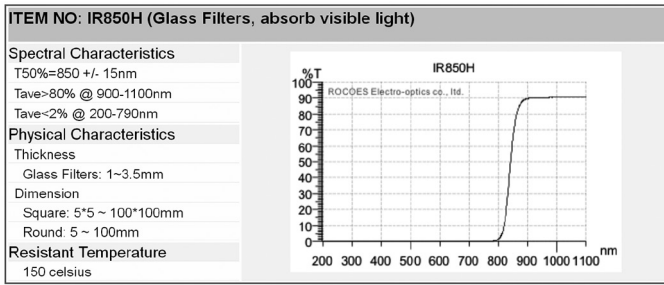


Fig. 4: Spectral characteristics of the IR 850H filter (RocoES 2015).

ister NIR radiation only. The experiment was based on the use of the IR 850H lens filter. Fig. 4 demonstrates the effect of this filter.

The combination of the characteristics demonstrated in Figs. 3 and 4, and a silicon sensitivity curve for the 1,000 nm – 1,100 nm curve from DARMONT (2009) has made it possible to determine the approximate relative spectral sensitivity of the camera (1) (Fig. 5):

$$\frac{Qr_{\lambda}}{Qr_{max}} = T_{\lambda} \cdot SR_{\lambda} \tag{1}$$

where: Qr_{λ} – The relative spectral sensitivity of the camera for a given wavelength, T_{λ} – Filter transmission (Fig. 4), and SR_{λ} – Spectral response (Fig. 3) for $\lambda < 1,000$ nm and for $\lambda > 1,000$ nm (DARMONT 2009, Fig. 5).

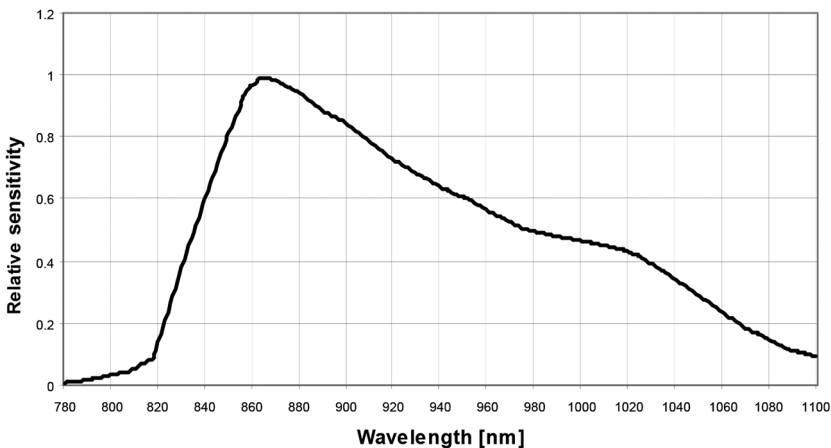


Fig. 5: The approximate relative spectral sensitivity of the modified camera.

The analysis of Fig. 5 makes it possible to conclude that the characteristics of the camera's sensitivity in the NIR region is not at optimum, because it has a wide range and lacks a strong peak.

3 Assumptions and Course of the Study

The studies conducted here had two objectives: (i) to verify the usefulness of a modified camera as an inexpensive research tool in geology and (ii) to determine the possibilities of using such a camera for a specific purpose, i.e., rock classification in the “Czatkowice” Limestone Mine.

The studies were conducted in several stages. The first stage involved the collection of typical samples of the rocks present in the

Czatkowice deposit, and their geological classification. This was followed by spectrometric observations of the samples under laboratory conditions in order to determine the spectral characteristics of the individual rock formations. The obtained spectral curves also enabled a preliminary assessment of rock separability in the channels used by the modified camera. The next stage included taking photographs of the samples under laboratory conditions and the following processing steps:

- Preparation of NIR pixel values for each sample and comparison of those values to the spectral curves.
- Determination of the pair-wise separability of the rock classes in the RGB and RGB+NIR channels, which is a key requisite for a correct classification.
- Supervised classification using the set of NIR, RGB and RGB+NIR data, and accuracy assessment.

The comparison of the brightness of NIR image pixels for the individual samples to the spectral curves will determine, if the camera is useful as a research tool. A strong dependence between those data will indicate that the sensitivity of the camera has been correctly determined (Fig. 5). The calculation of the pair-wise separability of classes for samples recorded on VIS+NIR photographs will, in turn, enable to assess the suitability of the method in the conditions of the Czatkowice limestone deposit. A significant increase of the pair-wise separability of classes for the set of RGB+NIR channels in relation to the RGB set will indicate the potential of the method for classifying the rocks in Czatkowice. The next stage of the study was the classification of the supervised samples of rocks using different VIS+NIR channels and assessment of its accuracy. The final stage was the verification of the method under field conditions for a fragment of the quarry wall. All of the stages listed above are described in detail in the following chapters.

4 Laboratory Tests of Rock Samples

The starting point was the results of the spectrometric studies of rock samples from the Czatkowice Limestone Mine, carried out by the author. The mine is located on the western slope of Krzeszowka Valley, in Czatkowice, approximately 20 km west of Cracow, in the south-western part of the Cracow-Czestochowa Upland. The geological characteristics of the study area are determined by its setting in the Krzeszowka Fault and Debnik Anticline, in the southern part of the Cracow-Silesia Monocline. The outcrops of the Czatkowice Quarry are marine sediments formed in the lower carboniferous era (Tournasian and Visean) and are represented by limestones and dolomites. In the sub-surface, particularly in the south section of the quarry deposits, sandy-clay sediments of the lower and middle Jurassic eras are prevalent, with Quaternary clay sediment cover (GRUDZIŃSKI 1972). The samples have been classified by a geologist as follows (Toś 2014) (Fig. 6):

- Sample 1 – limestone, dolomitic, microcrystalline, dark beige, slightly stromatolitic texture. This sample represents rock formations of Tournasian age which are the oldest within Czatkowice Quarry.
- Sample 2 – limestone, microcrystalline with heavily weathered surface, pink-dark-beige, stromatolitic texture, rock formations of Tournasian age.
- Sample 3 – limestone, microcrystalline, beige. Contains some fragments of silica and calcite crystals and veinlets partings, approximately 2 mm – 4 mm wide. Forms the main deposits extracted at the Czatkowice Quarry. Rock formations of Visean age.
- Samples 4 and 6 – limestone, microcrystalline, dark grey to black (bituminous limestone), stromatolitic texture. Rock formations of Tournasian age.
- Sample 5 – dolomitic limestone, microcrystalline, light to dark beige. Contains calcite crystals 1 mm in diameter and some calcite veinlets 2 mm – 3 mm wide. Latest rock formations of Tournasian age.



Fig. 6: Samples from the Czatkowice Limestone Mine: microcrystalline limestone (1); weathered limestone (2), (7); silicated limestone (3); bituminous limestone (4), (6); dolomitic limestone (5); sandstone (8); coarse crystalline calcite (9).

- Sample 7 – limestone, microcrystalline, rock formations of Visean age (represents the same rocks as sample 3). However, the study was carried out on a heavily weathered surface, dusky-red, creamy-brown.
- Sample 8 – quartz-sandstone, do not react with hydrochloric acid, heavily weathered, reddish-creamy-brown. Part of the late and middle Jurassic sandstone deposits.
- Sample 9 – calcite, cream-yellowish-brown. The calcite crystals are up to 10 cm high and 2 cm – 3 cm in diameter. Calcite is a mineral formed within Visean limestone as a result of intense karstification, creating approximately 10 cm wide, coarse-grained calcite veins.

The examination was carried out using the FIELD SPEC 3 in-field spectrometer. The spectral resolution of that device is 3 nm (in the 350 nm – 1,400 nm range) and 10 nm (in the 1,400 nm – 2,500 nm range), and it has a sampling interval of 1.4 nm to 2 nm. The field of view is 25 degrees. This enables reflectance recording in 2,151 channels in the 350 nm – 2,500 nm range. The study was conducted using two ASD lamps lighting the sample from both sides in relation to the position of the fibre-optic cable used for the measurement. The distance between the lamps and the samples was approximately 40 cm, and the distance from the detector was approximately 10 cm.

The fibre-optic cable and lamps were set not to cast a shadow on the measured samples. ASD lamps can focus or disperse the stream of the emitted light. During the experiment, they were set to an intermediate value. The instrument was calibrated using a white standard (spectralon). During the study, the same standard was also used for verification. The instrument was set to record reflectance. No additional spectral smoothing was done. 15 measurements were made for each sample at randomly selected points on the surfaces visible in Fig. 6. The measurement results (in the form of average values calculated based on observations) were presented in the form of spectral curves (Fig. 7).

The results of the spectrometric studies based on the analysis of the spectral curves registered for the samples indicate:

- There are no significant differences among the light reflection coefficients registered for limestones, dolomitic limestones, and silicated limestones (samples 1, 3, and 5).
- Bituminous limestones (samples 4 and 6) demonstrate a low light reflection coefficient in the entire VIS-NIR region, which facilitates their distinguishing.
- Weathered limestone (samples 2 and 7), coarse crystalline calcite (9), and sandstone (8) can be distinguished among all other limestone types in the R or NIR regions. Distinguishing these formations

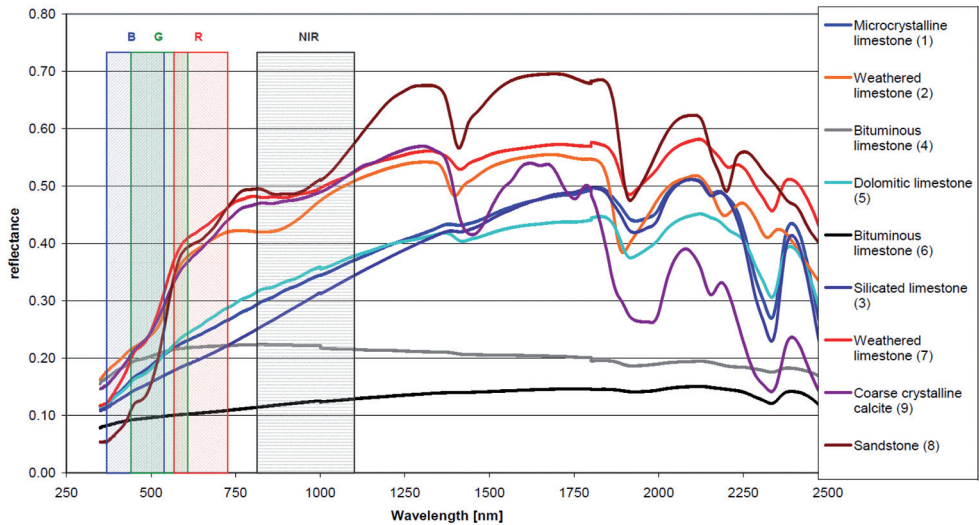


Fig. 7: Spectral curves of the studied dry samples (Toś 2014) and the R, G, B and NIR channel sensitivity ranges of the applied cameras.

from limestones is quite important, because they combined with soil overburden form the so-called ground-rock mass that is disposed to landfills.

Comparing the obtained spectral curves to the data of similar rock formations collected in USGS or ASTER spectral libraries (CLARK et al. 2007, BALDRIDGE et al. 2009) demonstrates that they are fairly atypical. This is caused by, among other factors, weathering of the minerals in samples 2 and 7, as well as surface oxidation of samples 1, 3, and 5. The shape of the spectral curves for the sandstone (8) and crystalline calcite (9) is, to a large extent, caused by the admixture of iron compounds (producing the characteristic coppery colour). The research has also proven that the moisture of rocks has a major impact on the reflection coefficient. This may influence the obtained classification results. The samples were soaked in water for 1 minute, pulled out and left for 3 minutes in order to remove excess water. Then, they were subject to observations. The examination method was the same as for the dry samples. The average values of the observations are indicated in Fig. 8.

Wet rocks have lower reflectance. A large change of the spectral curves is particularly noticeable for the weathered rocks and sandstone. Those formations have fairly high po-

rosity. The impact of moisture content on reflectance becomes particularly massive, in the area of water absorption spectra (around 1,950 nm, 1,450 nm, and 970 nm). Under good weather conditions the surface of the quarry wall in the Czatkowice Limestone Mine is dry. Therefore, photographs of nine dry samples were made in natural light, using a standard Nikon D5000 camera and a modified Nikon D200 camera with the IR 850H filter. All images were superimposed on each other, using the PI-3000 photogrammetry software. The RMS alignment error for images on twelve ground control points was 0.75 pixel. The photographs were subject to further studies.

5 Comparing the Brightness of Pixels Registered with the NIR Camera against the Spectral Curves of Samples

The suitability of the modified camera as a research tool can be verified, when we compare the images registered with the modified camera against the spectral characteristics of the analysed objects. In this case, it is necessary to obtain a strong correlation between those quantities.

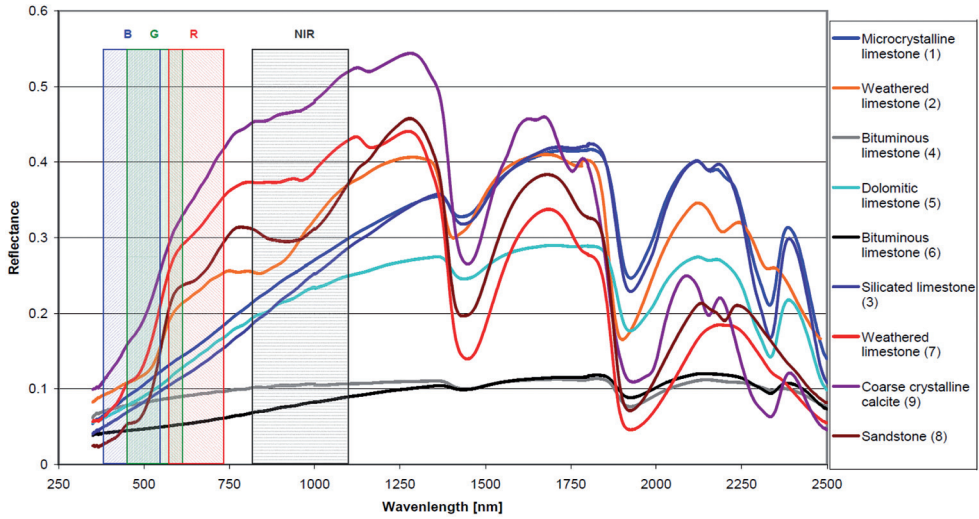


Fig. 8: Spectral characteristics of the wet samples (Toś 2014) with the channel ranges of the applied cameras.

It is difficult to find a relationship between the pixel value in an image and light reflection coefficients determined during spectrometric studies, because the charge-coupled device registers a wide range of radiation as demonstrated in Figs. 1 and 5. The spectral resolution of the spectrometer is 1 nm. According to the Lambertian image formation model, the camera's sensor response ρ to the light reflected by an object may be calculated on the basis of the following (2):

$$\rho = \int E(\lambda) \cdot S(\lambda) \cdot Q_s(\lambda) d\lambda \quad (2)$$

where $E(\lambda)$ is spectral power distribution (SPD) of light, which is incident upon the surface; $S(\lambda)$ denotes surface reflectance, and $Q_s(\lambda)$ sensor sensitivities. If only one image is analysed, it can be assumed that the $E(\lambda)$ function is constant for all samples. If spectrometer measurements of objects and the spectral sensitivity of the camera are known the $\rho_{i,j}$ coefficient calculated according to (3) is in proportion to the quantity of light reflected from the i -sample and registered by the detector in the j -band.

$$\rho_{i,j} = \sum_{\lambda_{\min}}^{\lambda_{\max}} \left(\frac{S_{\lambda,i} \cdot Q_{r,\lambda,j}}{\lambda_{\max} - \lambda_{\min}} \right) \quad (3)$$

where λ_{\min} and λ_{\max} constitute the minimum and maximum wavelength of light registered by the detector, while $S_{\lambda,i}$ is the light reflection coefficient of the each sample registered by the spectrometer for a given wavelength. $Q_{r,\lambda,j}$ is the relative spectral sensitivity of the camera in the j -band for a given wavelength (Figs. 1 and 5).

The $\rho_{i,j}$ coefficient was calculated for all samples. Fig. 9 demonstrates the relationship between the mean pixel value of each sample and the $\rho_{i,j}$ coefficient for the NIR and R channels. The study suggests that there is a strong correlation between those quantities. The determination coefficients for the NIR and R channels are 0.92 and 0.85, respectively.

6 Suitability of the Modified Camera for Classifying Rocks at the Czatkowice Limestone Mine

The verification of the thesis that a modified camera can be used to classify rock formations at the Czatkowice Limestone Mine consisted in the comparison of the separability factor for pairs of classes against different sets of spectral bands. The obtained images made it possible to define nine classes corresponding

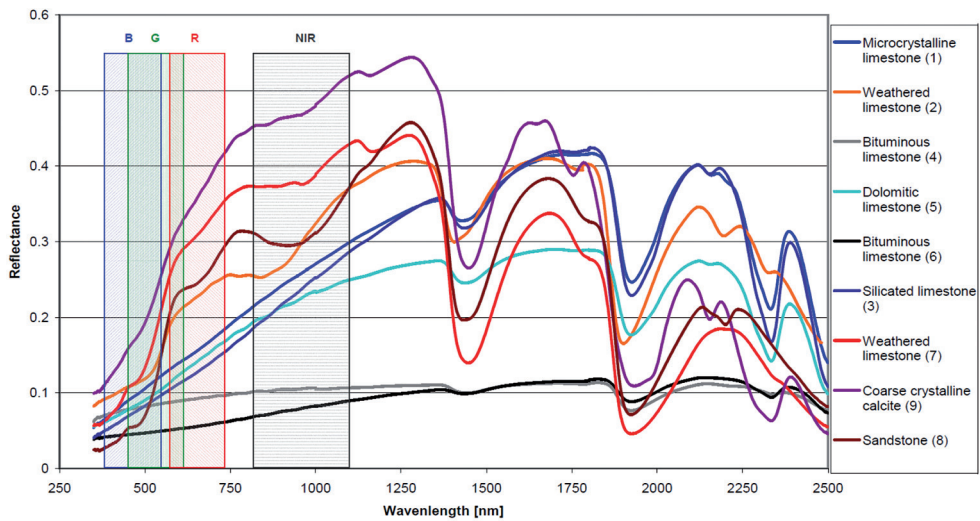


Fig. 9: Comparison between mean value of sample pixels against the ρ_1 coefficient for the *NIR* and *R* bands.

to each of the samples. The separability factor was determined for all pairs of classes, in the form of transformed divergence (TD), in the RGB, GB+NIR, RB+NIR, RG+NIR, and RGB+NIR band sets (Tab. 1). This coefficient gives results in the range from 0 to 2,000. Any value above 1,600 indicates good separability (RICHARDS 1993).

The overall TD values exceeding 1,600 for each set of channels show good separability for all combinations (Tab. 1). The best sepa-

rability factor for samples was achieved when the analysis was carried out for the full set of 4 channels. A slightly better separability in relation to the RGB channel set could also be obtained by replacing the red channel (R) or green channel (G) with the infrared channel (NIR). Furthermore, when analysing TD values for each pair of classes, one can notice that none of the analysed sets of channels could statistically separate the following pairs of samples (Tab. 1):

Tab. 1: Transformed divergence coefficient (TD) for selected pairs of samples.

Pair of samples	Bands				
	RGB	GB+NIR	RB+NIR	RG+NIR	RGB+NIR
1 – 3	862	940	1,002	839	1,108
4 – 6	644	716	661	727	867
7 – 9	845	814	897	845	923
2 – 9	1,909	1,794	1,540	1,233	1,921
3 – 5	1,950	1,821	1,964	1,738	1,967
1 – 4	1,142	1,990	1,989	1,992	1,993
1 – 6	1,368	1,982	1,981	1,980	1,985
3 – 4	1,613	1,979	1,994	1,988	1,995
3 – 6	1,528	1,917	1,967	1,938	1,969
Overall TD	1,823	1,878	1,874	1,819	1,905

- 1 – 3 (microcrystalline limestone – limestone);
- 4 – 6 (bituminous limestone – bituminous limestone);
- 7 – 9 (weathered limestone – calcite).

The low TD values for the first two pairs can be attributed to the similar composition of the samples; for the third pair, the similarity is due to the presence of iron compounds resulting in the similar spectral characteristics of both rocks in the considered bands. When the R channel is replaced with the NIR channel, the separability factor is reduced for the following pairs: 2 – 9 (weathered limestone – calcite) and 3 – 5 (dolomitic limestone – limestone), while the TD coefficient is increased significantly for the following pairs (Tab. 1):

- 1 – 4 (microcrystalline limestone – bituminous limestone);
- 1 – 6 (microcrystalline limestone – bituminous limestone);
- 3 – 4 (limestone – bituminous limestone) and
- 3 – 6 (limestone – bituminous limestone).

If all four channels are included in the analysis, the TD coefficient is increased for all pairs of classes, when compared with the RGB channel set.

7 Classification of Rock Samples

The analysis of TD values, spectral curves and the mineral composition of limestone samples lead to the conclusion that it is extremely difficult to distinguish between limestones and dolomitic or silicated limestones. This is due to the small admixtures of dolomite and silica and the limited diagnostic capabilities in the channels which were used for the analysis of those formations. In these circumstances, limiting the number of classes to the 5 basic types, i.e., limestones (samples 1, 3, and 5), bituminous limestones (samples 4 and 6), sandstone

(sample 8), coarse crystalline calcite (sample 9), and weathered limestone (samples 2 and 7) should increase the reliability of the classification. The classification of basic rock types was carried out for three sets of channels (RGB, GB+NIR, and RGB+NIR), using the MLC technique (Maximum-Likelihood Classification, RICHARDS 1993). However, this method is sensitive to various light conditions. Consequently, a similar classification was done using the spectral angle mapper (SAM) method. This method is not affected by solar illumination factors (KRUSE et al. 1993). The SAM classification uses the same training polygons as in the MLC method, and the angle threshold of classification was specified as 20 deg. The results of the analyses were compared with prepared true images. Tab. 2 presents the kappa index of agreement (KIA) that determines the accuracy of the classification (ROSENFELD & FITZPATRICK-LINS 1986). Fig. 10 demonstrates a comparison between truth images and the results of the classification carried out for different methods and sets of channels.

The results of the classification greatly improved, when the NIR channel was applied. The best KIA was achieved for the set of four channels. In the MLC (Fig. 10 b, c) there is a noticeable adverse impact of sample illumination. But the SAM method produced less favourable results (Fig. 10 d, e). The impact of illumination was reduced (which is particularly noticeable in the case of the sandstone), but classification errors occurred particularly for samples with a non-uniform surface (weathered limestone and coarse crystalline calcite).

8 Verification of the Method in Field Conditions

Besides testing under laboratory conditions, some preliminary actions were taken to verify the method in field conditions. The subject

Tab. 2: KIA (kappa index of agreement) for the MLC and SAM classifications of the basic rock types based on various sets of bands.

Bands	RGB	GB+NIR	RGB+NIR
MLC overall kappa	0.7550	0.8095	0.8375
SAM overall kappa	0.4980	0.5816	0.6299

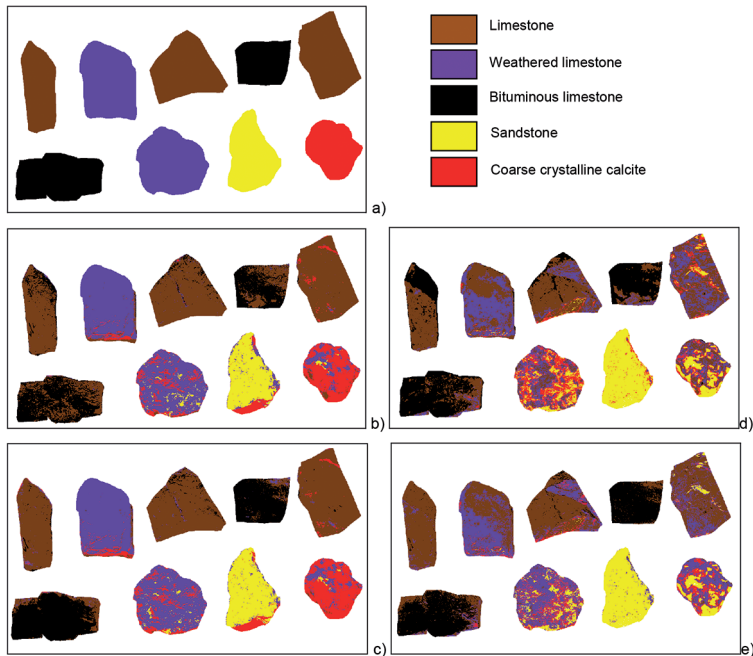


Fig. 10: Classification of the main rock types: True image (a) and classification results: b) MLC based on the RGB channels, c) MLC based on the RGB+NIR channels, d) SAM classification based on the RGB channels, e) SAM classification based on the RGB+NIR channels.

of examination is a fragment of a quarry wall (Figs. 11 and 12) with the following rock formations identified around its area: limestones, bituminous limestone, coarse crystalline calcite, which is the main component of karst formations, and additionally some shales.

The photographs were recorded on the 15th of September at 11:00 am under cloudless skies. Dry weather conditions before image acquisition ensured minimal moisture content of the rocks. The photographs were taken 15 m away from the quarry wall. A geological classification of wall fragments was performed. The places subject to classification were marked with paint so that they could later be used for the definition of the training polygons in the classification (Fig. 13).

One of the significant differences between field and laboratory conditions is lighting. The surface of the quarry wall was highly irregular, which resulted in overshadowing a great portion of the surface, if exposed to the sun. The removal of the shadow from the images becomes possible with the use of methods

commonly implemented in satellite remote sensing. For example, GILES (2001) suggested an automatic shadow detection algorithm, based on the geometric properties of the terrain. In the case of a quarry wall, it is required to carry out an additional measurement, using photogrammetry or laser scanning, in order to acquire information about its geometry. Another method to detect and remove shadows from images consists in a radiometric analysis of the properties of image fragments (DARE 2005). However, because no shadow correction could be implemented at this phase of research due to the absence of the required additional information shadows or irregularly illuminated parts of wall were excluded by permitting the presence of unclassified pixels in the classification. Properly defined training polygons made it possible to count all the pixels located in the shaded areas as unclassified (Fig. 14).

Unshaded areas on an irregular quarry wall are also characterized by a certain variability of illumination. That impact can be limited

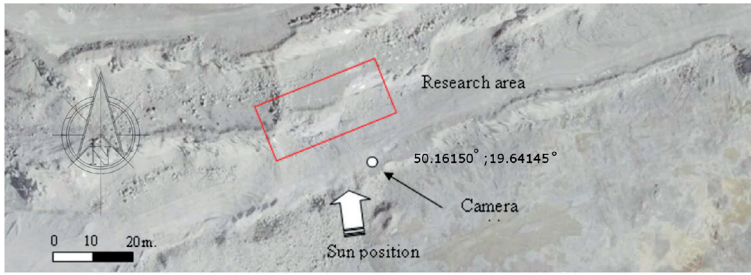


Fig. 11: Location of the examined object.



Fig. 12: Fragment of the quarry wall – image in the NIR channel.

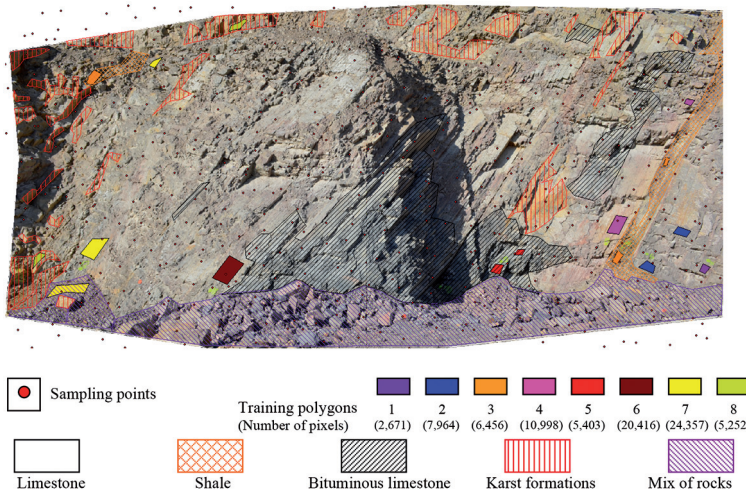


Fig. 13: Geological classification of the quarry wall, sampling points and training fields for the classification. 1: microcrystalline limestone with wavy texture, grey-brown (creamy); 2: microcrystalline limestone, uniform, cream-coloured, with black cherts with a height of 3 cm – 5 cm; 3: shale, brown with weathered light-olive layers (presence of brown clay); 4: microcrystalline limestone, pink, stromatolitic texture; 5: microcrystalline bituminous limestone, uniform texture, dark grey to black; 6: creamy microcrystalline limestone, uniform, hard, with dark grey cherts with a height of 5 cm – 7 cm and a length of over a dozen cm, parallel to stratification; 7: microcrystalline limestone, grey, with a slight tint of brown, uniform texture; 8: coarse crystalline calcite, colourless, and with a weathered coppery-yellow surface.

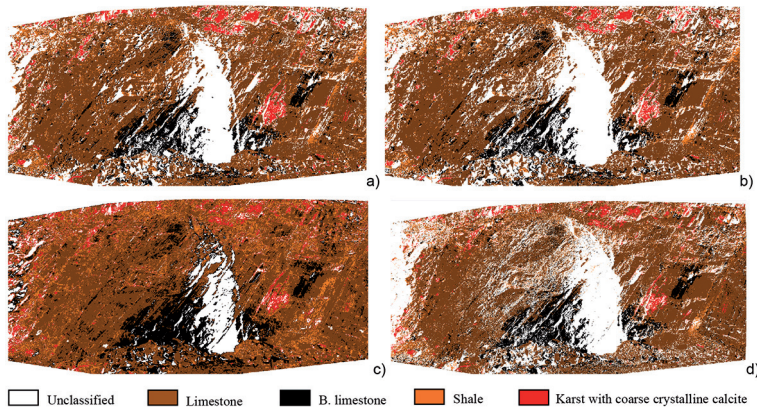


Fig. 14: Classifications results for rock formations a) MLC method based on RGB channels; b) MLC method based on RGB+NIR channels; c) SAM method based on RGB channels; d) SAM method based on RGB+NIR channels.

using a method that is less susceptible to that variability, e.g. SAM. For assuring the comparability to the laboratory tests, two methods were used to classify the formations in the deposit: MLC and SAM.

The same training polygons were used for both methods. Eight classes defined by the geologist were reduced to four basic types of rocks (Fig. 12): Limestone (classes: 1, 2, 4, 6, 7); Shale (class 3); Bituminous limestone (class 5); Karst with coarse crystalline calcite (class 8). For MLC, in order to eliminate the highly shaded areas, 10% of unclassified pixels were allowed, and in the SAM method the maximum classification angle was specified to be 3 degrees. The classification results are presented in Fig. 14.

The classification was verified based on 500 control points. Stratified random sampling was used. The strata were defined on the basis of initial classification of the quarry wall (Fig. 13). After this, control points, were verified geologically during a site inspection. The number of control points in the strata amounted to: Limestone -337, Bituminous limestone -80, Karst with coarse crystalline calcite -31, Shale -19, Background -36. Unfortunately some of points were located in unclassified areas (Fig. 14). The classification accuracy and KIA were determined for the remaining (Tabs. 3 and 4).

Unlike in the laboratory conditions, both classification methods exhibited similar accuracy. One of the causes are the illumination conditions (to which the MLC is very susceptible), which were less favourable than in the laboratory. In both cases, the accuracy of classification was slightly better, when an additional NIR channel was used. However, a more in-depth analysis of results leads to the conclusion that the increased accuracy of classification was to a large extent caused by the fact that some of the incorrectly classified pixels are not classified at all after the inclusion of the NIR channel into classification.

Upon consideration of the individual rocks, it can be observed that:

- For Karst formations containing coarse crystalline calcite, the introduction of the NIR channel does not result in a relevant change of classification accuracy (Fig. 15 a).
- NIR improved the identification of bituminous limestone in the two methods (Fig. 15 b).
- The numerical data in Tabs. 4 and 5 indicate a large error of shale classification, as confirmed by the reference images (Fig. 16 a and b), although a certain improvement is noticeable in the MLC after the introduction of the NIR channel.

Tab. 3: Accuracy of the MLC classifications.

RGB channels					
classification \ True	Limestone	Shale	Bituminous limestone	Calcite	Total
Limestone	215	41	10	6	272
Shale	7	4	0	0	11
Bituminous limestone	11	3	28	0	42
Calcite	2	2	0	16	20
Total	235	50	38	22	345
Classification accuracy 0.76, KIA 0.46					
Classification accuracy 0.80, KIA 0.54 – for all (305) control points which remained classified for each method.					
RGB+NIR channels					
classification \ True	Limestone	Shale	Bituminous limestone	Calcite	Total
Limestone	214	30	11	3	258
Shale	5	5	0	0	10
Bituminous limestone	7	2	32	0	41
Calcite	2	1	0	13	16
Total	228	38	43	16	325
Classification accuracy 0.81, KIA 0.56					
Classification accuracy 0.84, KIA 0.59 – for all (305) control points which remained classified for each method.					

9 Discussion

The results obtained in the field investigations are of reduced accuracy in comparison to those received under laboratory conditions. In order to determine the reasons, it is necessary to begin with an in-depth analysis of the laboratory results. None of the examined rock formations exhibits diagnostic spectral features at least for the wide channels recorded by the camera. Under such conditions, rock classification is based on differences in the general albedo of the individual formations. The spectral curves in Fig. 7 indicate that the limestones present in the deposit have very similar characteristics, which prevents them from being distinguished within the sensitivity ranges of the cameras. Exceptions from this are bituminous limestones, which have low reflectance in RGB and NIR channels. Other formations in the deposit and weathered limestone demonstrate much higher reflection coefficients

in R and NIR channels than limestone, which enables their discrimination during laboratory tests. However, the examined surfaces of the samples depicted in Fig. 6 have a fairly uniform structure. Under natural conditions, the degree of weathering or oxidation of the limestone surface is highly variable. Classification based on differences in the general albedo of the individual formations would then produce much worse results. An additional factor present under natural conditions is the fineness of the material. The pixel value recorded by the camera depends on the reflection of light from multiple small grains. This problem is referred to as spectral mixture (GIROUARD et al. 2004). It is particularly noticeable in the classification of shale using the SAM method (Fig. 16b). SAM is susceptible to this phenomenon. In places, where considerable fragmentation of rocks is present, there are high local variations in the spectral property of a surface resulting from, for instance, shading effects, humidity

Tab. 4: Accuracy of the SAM classifications.

RGB channels					
classification \ True	Limestone	Shale	Bituminous limestone	Calcite	Total
Limestone	237	43	24	13	317
Shale	13	3	0	1	17
Bituminous limestone	19	3	41	0	63
Calcite	5	3	1	18	27
Total	274	52	66	32	424
Classification accuracy 0.71, KIA 0.39					
Classification accuracy 0.76, KIA 0.45 – for all (305) control points which remained classified for each method.					
RGB+NIR channels					
classification \ True	Limestone	Shale	Bituminous limestone	Calcite	Total
Limestone	207	23	14	9	253
Shale	9	7	0	0	16
Bituminous limestone	6	1	35	0	42
Calcite	3	1	0	14	18
Total	225	32	49	23	329
Classification accuracy 0.80, KIA 0.55					
Classification accuracy 0.81, KIA 0.56 – for all (305) control points which remained classified for each method.					

fluctuations and rock material displacements. These variations caused that these areas have been wrongly classified as shales.

In the investigated area Karst formations occur which develop along faults. They have the form of coarse crystalline calcite veins and dripstones. They are accompanied by a concentration of iron compounds that give them a specific colour. Dripstones are composed of cryptocrystalline or fine crystalline calcite, with colour ranging from white to yellow-brown. The dripstones are present in the vicinity of calcite veins, and they may also cover limestone. Classification using surface imaging does not enable distinguishing between the rocks present under those dripstones. This can be done only by directly examining the rocks.

The comparison of the obtained results to other similar studies should begin with the study that is most similar (Toš 2014). That

study concerned the use of scanning data from terrestrial laser scanner (TLS) for the classification of the same rock samples. In that paper, photographs in the RGB channels were also used, but the intensity of laser beam reflection (I) was recorded instead of the NIR channel in modified camera. The correlation between the spectral curves and I value is lower (coefficient of determination $R^2 = 0.65$) than that obtained in this study for the NIR channel ($R^2 = 0.92$). The accuracy of classification using the RGB+I data from TLS operating with a wavelength of 785 nm was also inferior (KIA = 0.77) to the accuracy achieved in the presented paper (KIA = 0.83). Better values were reported by FRANCESCHI et al. (2009) investigating the dependence between the intensity of laser beam reflection (1,535 nm) and clay abundance in the quarry wall of the limestone mine. The coefficient of determination was 0.85. Those values indicate that the use of

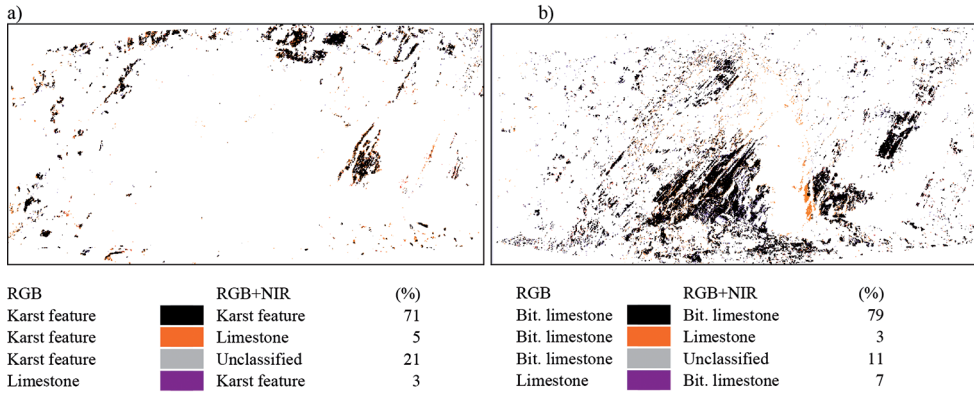


Fig. 15: Comparison of MLC classifications using RGB and RGB+NIR channels: a) for Karst formations containing coarse crystalline calcite; b) for bituminous limestone.

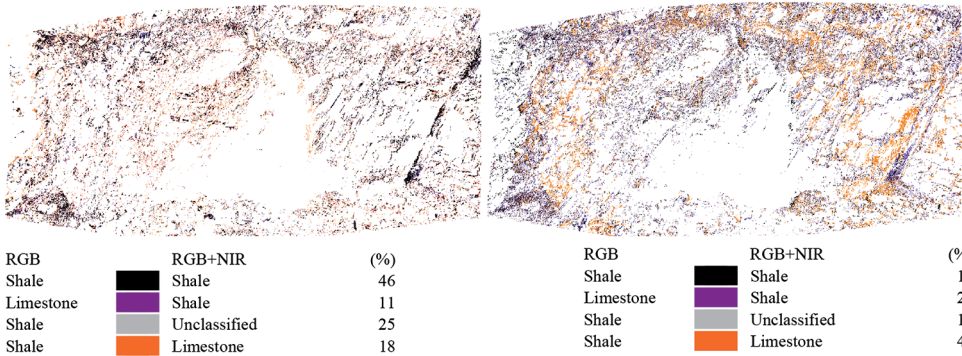


Fig. 16: Comparison of shale classifications using RGB and RGB+NIR channels: a) MAXLIKE; b) SAM.

a modified camera may produce results comparable to scanning data. On the other hand, PATEL & CHATERIEE (2016) presented a method of limestone classification with an impressive accuracy (classification accuracy = 0.94). That method only uses photographs in the RGB channels. The authors achieved such a high accuracy owing to the use of a probabilistic neural network and, which is equally important, performance of the tests under controlled laboratory conditions using samples that were collected already after blasting works. This eliminated other interfering factors that had such a large impact on the results obtained in this study.

10 Conclusions

Charge-coupled devices in digital camera are sensitive for near infrared. It is considered a flaw in the majority of cases and manufacturers install appropriate filters, in order to counteract that. When such filters are eliminated, it is possible to register light in the entire visible spectrum, and additionally in the 780 nm – 1,100 nm range. The sensitivity characteristics of the modified camera in the NIR region are not as good as of the equipment designed for that purpose alone. The primary flaw is the wide range of the RGB and NIR channels. However, the images registered with such a device can provide some valuable data. Alternatively, it is possible to apply special tools,

e.g. ground-based hyper-spectral cameras, although they are far more expensive.

The article targeted the possibility of classifying rock formations at the Czatkowice Limestone Mine using the modified camera. The tests were carried out in laboratory conditions and with stable lighting, making sure that the humidity level of the samples was at its minimum. In such conditions, it was possible to obtain a strong correlation ($R^2 = 0.92$) between the brightness of the pixels registered with the modified camera and the results of spectrometric observations of rock samples. Furthermore, it was proven that the results of classification for the rock formations present in the deposit were improved, when the R channel was replaced with the NIR channel. It is particularly advantageous to apply a full set of RGB+NIR channels, as it will result in a high level of classification accuracy (KIA 0.83).

However, the tests carried out in field conditions returned worse results. The accuracy of rock classification was KIA = 0.56, when using the RGB+NIR set of channels. Still, the final result was better, than the one obtained for the classification based on RGB channels (KIA = 0.46). It depends on a number of factors. They include, among others, changeable lighting conditions and various levels of weathering, oxidation, grain size and humidity, concerning the rock formations present in the deposit, as well as surface contamination. In the Czatkowice Limestone Mine, where the rock formations have very similar spectral characteristics, the above-mentioned factors have a decisive impact on the correctness of classification. This limits the possibilities of using that solution to mapping rock formation in the quarry wall of that mine. However, this does not prevent the modified camera from being useful in the tests of rocks with other spectral characteristics in the VIS+NIR range.

Acknowledgements

I would like to express my gratitude to the Management of the Czatkowice Limestone Mine for the possibility of carrying out the tests, and to RAFAŁ GWOZDZ, Ph.D. (Eng.), for the geological verification of the samples.

References

- ASADZADEH & DE SOUZA FILHO, C.R., 2016: A review on spectral processing methods for geological remote sensing. – *International Journal of Applied Earth Observation and Geoinformation* **2016** (47): 69–90; doi: 10.1016/j.jag.2015.12.004.
- BALDRIDGE, A.M., HOOK, S.J., GROVE, C.I. & RIVERA, G., 2009: The ASTER Spectral Library Version 2.0. – *Remote Sensing of Environment* **2009** (113): 711–715.
- BONGIORNO, D.L., BRYSON, M., DANSEREAU, D.G. & WILLIAMS, S.B., 2013: Spectral characterization of COTS RGB cameras using a linear variable edge filter. – *SPIE Digital Photography* **9** (86600N), Burlingame, CA, USA; doi:10.1117/12.2001460.
- BROWN, A.J., 2006: Spectral curve fitting for automatic hyperspectral data analysis. – *IEEE Transactions on Geoscience and Remote Sensing* **44**: 1601–1608.
- CHATTERJEE, S., BHATTACHERJEE, A., SAMANTA, B. & PAL, S.K., 2010: Image-based quality monitoring system of limestone ore grades. – *Computers in Industry* **16**: 391–408.
- CHEN, X., WARNER, T.A. & CAMPAGNA, D.J., 2007: Integrating visible, near-infrared and short-wave infrared hyperspectral and multispectral thermal imagery for geological mapping at Cuprite, Nevada. – *Remote Sensing of Environment* **2007** (110): 344–356; doi:10.1016/j.rse.2007.03.015.
- CIAMPALINI, A., GARFAGNOLI, F., ANTONIELLI, B., MORETTI, S. & RIGHINI, G., 2012: Remote sensing techniques using Landsat ETM+ applied to the detection of iron ore deposits in Western Africa. – *Arabian Journal of Geoscience* **6** (11): 4529–4546; doi: 10.1007/s12517-012-0725-0.
- CLARK, R.N., SWAYZE, G.A., WISE, R., LIVO, E., HOFEN, T., KOKALY, R. & SUTLEY, S.J., 2007: USGS digital spectral library splib06a. – U.S. Geological Survey, Digital Data Series **231**; <http://speclab.cr.usgs.gov/spectral.lib06>. (10.6.2015).
- DARE, P.M., 2005: Shadow analysis in high-resolution satellite imagery of urban areas. – *Photogrammetric Engineering & Remote Sensing* **71** (2): 169–177; doi: <http://dx.doi.org/10.14358/PERS.71.2.169>.
- DARMONT, A., 2009: Spectral Response of Silicon Image Sensors. – White paper; <http://www.aphesa.com/downloads/download2.php?id=1> (10.6.2015).
- EDWARDS, H.G.M., VILLAR, S.E.J., JEHLICKA, J. & MUNSHI, T., 2005: FT-Raman spectroscopic study of calcium-rich and magnesium-rich carbonate minerals. – *Spectrochimica Acta Part A* **2005** (61): 2273–2280; doi: 10.1016/j.saa.2005.02.026.
- FRANCESCHI, M., TEZA, G., PRETO, N., PESCI, A., GALLAGRO, A. & GIRARDI, S., 2009: Discrimination between marls and limestones using intensity data from terrestrial laser scanner. – *ISPRS Journal of*

- Photogrammetry and Remote Sensing **64** (6): 522–528; doi: 10.1016/j.isprsjprs.2009.03.003.
- FREDEMBACH, C. & SUSSTRUNK, S., 2009: Illuminant Estimation and Detection Using Near infrared. – IS&T/SPIE Electronic Imaging, Digital Photography **5** (7250): 18–22, San Jose, CA, USA.
- GILES, P., 2001: Remote sensing and cast shadows in mountainous terrain. – Photogrammetric Engineering & Remote Sensing **67** (7): 833–839.
- GIROUARD, G., BANNARI, A., EL HARTI, A. & DESROCHERS, A., 2004: Validated spectral angle mapper algorithm for geological mapping: comparative study between quickbird and landsat-tm. – XXth ISPRS Congress, Geo-Imagery Bridging Continents **2004**: 12–23, Istanbul, Turkey.
- GOETZ, A.F.H., 2009: Three decades of hyperspectral remote sensing of the Earth: a personal view. – Remote Sensing Environment **2009** (113): 5–16; doi: 10.1016/j.rse.2007.12.014.
- GRUZINSKI, R., 1972: Przewodnik geologiczny po okolicach Krakowa. – Polish Geological Publishing House, Warsaw, Poland.
- HAEST, M., CUDAHY, T., LAUKAMP, C. & GREGORY, S., 2012: Quantitative mineralogy from infrared spectroscopic data. I. Validation of mineral abundance and composition scripts at the Rocklea channel iron deposit. – Economic Geology **2012** (107): 209–228; doi: 10.2113/econgeo.107.2.209.
- HUNT, G.R., 1977: Spectral signatures of particulate minerals in the visible and nearinfrared. – Geophysics **42** (3): 501–513; doi: 10.1190/1.1440721.
- HUNT, G.R., 1980: Electromagnetic radiation: The communication link in remote sensing. – SIEGAL, B.S. & GILLESPIE, A.R. (eds.): Remote sensing in geology, 5–45, John Wiley, New York, NY, USA.
- KOVACEVIC, M., BAJAT, B., TRIVIC, B. & PAVLOVIC, R., 2009: Geological Units Classification of Multi-spectral Images by Using Support Vector Machines. – Intelligent Networking and Collaborative Systems, International Conference ICONOS **2009**: 267–272; doi: 10.1109/INCOS.2009.44.
- KRUSE, F.A., BOARDMAN, J.W., LEFKOFF, A.B., HEIDEBRECHT, K.B., SHAPIRO, A.T., BARLOON, P.J. & GOETZ, A.F.H., 1993: The Spectral Image Processing System (SIPS) – Interactive Visualization and Analysis of Imaging Spectrometer Data. – Remote Sensing of Environment **44**: 145–163.
- KRUSE, F.A., 2015: Comparative analysis of airborne visible/infrared imaging spectrometer (AVIRIS), and hyperspectral thermal emission spectrometer (HyTES) longwave infrared (LWIR) hyperspectral data for geologic mapping – Algorithms and Technologies for Multispectral, Hyperspectral, and Ultraspectral Imagery XXI. – SPIE 9472: 94713–94727; doi: 10.1117/12.2176646.
- KUOSMANEN, V.V. & LAITINEN, L.J., 2008: Quantitative mineral assessment of apatite, calcite/dolomite, and phlogopite powder mixtures by using VSWIR reflectance. Geosci. – Remote Sensing IEEE Transactions **46**: 1774–1782.
- LEPISTO, L., KUNTTU, I. & VISA, A., 2005: Rock image classification using color features in Gabor space. – Journal of Electronic Imaging **14** (4): 040503-040503-3; doi: http://dx.doi.org/10.1117/1.2149872.
- LIU, E., SONG, Y., WANG, H., LIU, H., AYOKO, G.A., FROST, R.L. & XI, Y., 2016: Vibrational spectroscopic characterization of mudstones in hydrocarbon-bearing depression, South China Sea: Implications for thermal maturity evaluation. – Spectrochimica Acta Part A: Molecular and Biomolecular Spectroscopy **153**: 241–248; doi: 10.1016/j.saa.2015.08.031.
- MAXMAX, 2015: https://www.maxmax.com/spectral_response.htm (13.5.2015).
- MENGKO, T.R., SUSILOWATI, Y., MENGKO, R. & LEKSONO, B.E., 2000: Digital image processing technique in rock forming minerals identification. – Circuits and Systems 2000, IEEE APCCAS 2000, The 2000 IEEE Asia-Pacific Conference **2000**: 441–444, Tianjin, China; doi: 10.1109/APCCAS.2000.913531.
- NAKAMURA, J., 2006: Image Sensors and Signal Processing for Digital Still Cameras. – Taylor & Francis, Boca Raton, FL, USA.
- NIKOND200, 2015: http://www.image-engineering.de/library/tests/nikon_d200_spectral_sensitivities.pdf (12.5.2015).
- NIKOND70, 2015: http://www.lifepixel.com/tutorials/infrared-diy-tutorials/nikon-d70-d70s (10.6.2015).
- NURDAN, A.B. & NIHAT, Y., 2010: Mineral identification using color spaces and artificial neural networks. – Computers & Geosciences **36** (1): 91–97; doi: http://dx.doi.org/10.1016/j.cageo.2009.04.009.
- PATEL, A.K. & CHATERIEE, S., 2016: Computer vision-based limestone rock-type classification using probabilistic neural network. – Geoscience Frontiers, Progress of Machine Learning in Geosciences **7** (1): 53–60; doi: 10.1016/j.gsf.2014.10.005.
- PENASA, L., FRANCESCHI, M., PRETO, N., TEZA, G. & POLITO, V., 2014: Integration of intensity textures and local geometry descriptors from Terrestrial Laser Scanning to map chert in outcrops. – ISPRS Journal of Photogrammetry and Remote Sensing **93**: 88–97; doi: 10.1016/j.isprsjprs.2014.04.003.
- PIRARD, E., 2004: Multispectral imaging of ore minerals in optical microscopy. – Mineralogical Magazine **68**: 323–333; doi: 10.1180/0026461046820189.
- ROCOES, 2015: http://rocoes.com.tw/dichroic/optical/coldmiro.htm (6.6.2015).
- RICHARDS, J.A., 1993: Remote Sensing Digital Image Analysis. – Springer-Verlag, New York, NY, USA.

- ROSENFELD, G.H. & FITZPATRICK-LINS, K., 1986: A Coefficient of Agreement as a Measure of Thematic Classification Accuracy. – *Photogrammetric Engineering and Remote Sensing* **52** (2): 223–227.
- SULISTIYANTI, S.R., SETYAWAN, A. & SUSANTO, A., 2009: Histogram Characterizations of Infrared Images Captured by a Modified Digital Camera. – *International Journal of Electronic Engineering Research (IJEER)* **1** (4): 329–336, Research India Publications (RIP), ISSN 0975 – 6450.
- SULISTIYANTI, S.R., WIDODO, T.S., SUSANTO, A. & SUPARTA, G.B., 2010: Noise Filtering on Thermal Images Acquired by Modified Ordinary Digital Camera. – *International Conference on Electronics and Information Engineering (ICEIE 2010)* **2**: 462–464, Kyoto, Japan, ISBN 978-1-4244-7679-4; doi: 10.1109/ICEIE.2010.5559817.
- SULISTIYANTI, S.R., KOMARUDIN, M., HAKIM, L. & YUDAMSON, A., 2014: Study of environmental condition using wavelet decomposition based on infrared image. – *International Conference on Information Technology, Computer and Electrical Engineering (ICITACEE)* **1**: 172–176, Semarang, Indonesia, ISBN 978-1-4799-6431-4; doi: 10.1109/ICITACEE.2014.7065736.
- TARQUINI, S. & FAVALLI, M.A., 2010: Microscopic information system (MIS) for petrographic analysis. – *Computers & Geosciences* **36** (5): 665–674; doi: 10.1016/j.cageo.2009.09.017.
- THEUWISSEN, A.J.P., 1995: *Solid-State Imaging with Charge-Coupled Devices*. – Kluwer Academic Publishers, Dordrecht, The Netherlands.
- Toś, C., 2014: The possibilities of using the terrestrial scanning data for classification of rocks in limestone mine “Czatkowice” – Reports on Geodesy and Geoinformatics **97**: 80–90, Warsaw, Poland; doi: 10.2478/rgg-2014-0013.
- TURNER, D., BENOIT, R. & GROAT, L.A., 2014: Visible and short-wave infrared reflectance spectroscopy of REE fluorocarbonates. – *American Mineralogist* **99**: 1335–1346; doi:10.2138/am.2014.4674.
- VERHOEVEN, G., 2008: Imaging the invisible using modified digital still cameras for straightforward and low-cost archaeological near-infrared photography. – *Journal of Archaeological Science* **35** (12): 3087–3100, Elsevier, ISSN 0305-4403; <http://dx.doi.org/10.1016/j.jas.2008.06.012>.
- VAN DER MEER, F.D., VAN DER WERFF, H.M.A., VAN RUITENBEEK, F.J.A., HECKER, C.A., BAKKER, W.H., NOOMEN, M.F., VAN DER MEIJDE, M., CARRANZA, E.J.M., DE SMETH, J.B. & WOLDAL, T., 2012: Multi- and hyperspectral geologic remote sensing: A review. – *International Journal of Applied Earth Observation and Geoinformation* **14** (1): 112–128; doi: <http://dx.doi.org/10.1016/j.jag.2011.08.002>.

Address of the Author:

Ph.D eng. CEZARY Toś, Institute of Geotechnics S-2, Cracow University of Technology, ul. Warszawska 24, 31-155 Kraków, Poland, phone: +48 12 628-28-68, e-mail: ctos@wis.pk.edu.pl

Manuskript eingereicht: Februar 2016
Angenommen: Juli 2016